Molecular Cancer Therapeutics

2-Deoxy-Glucose Downregulates Endothelial AKT and ERK via Interference with N-Linked Glycosylation, Induction of Endoplasmic Reticulum Stress, and GSK3β Activation

Krisztina Kovács[1], Christina Decatur[2], Marcela Toro[1], Dien G. Pham[2], Huaping Liu[3], Yuqi Jing[1], Timothy G. Murray[2], Theodore J. Lampidis[3], and Jaime R. Merchan[1]

Abstract

Interference with endothelial cell metabolism is a promising, yet unexploited strategy for angiogenesis inhibition. We reported that the glucose analogue 2-deoxy-D-glucose (2-DG) inhibits angiogenesis at significantly lower concentrations than those required for tumor cytotoxicity. Here, we found that hypersensitivity to 2-DG in endothelial cells is not associated with enhanced drug uptake compared with tumor cells, but with time-dependent, endothelial-selective inhibition of AKT and ERK phosphorylation. Downregulation of these critical survival pathways is shown to be due to 2-DG's interference with N-linked glycosylation, leading to alterations in VEGFR2 (and downstream signaling) as well as induction of endoplasmic reticulum (ER) stress, GSK3β activation, and apoptosis. *In vivo*, periocular administration of 2-DG in $LH_{BETA}T_{AG}$ mice was associated with significant reduction of newly formed ($CD105^{+}$) tumor capillaries, ER stress (GRP 78 expression), and endothelial apoptosis (TUNEL). These findings uniquely link N-linked glycosylation inhibition, ER stress, and ERK/AKT downregulation in endothelial cells, and provide a novel drug development strategy to overcome resistance mechanisms to currently available antiangiogenic agents. *Mol Cancer Ther; 15(2); 264–75. ©2015 AACR.*

Introduction

The understanding of tumor angiogenesis and subsequent development of vascular-targeted agents have revolutionized the treatment of cancer (1). These agents improve clinical outcomes in patients with advanced renal cell carcinoma, colon, lung, and brain cancers (2–5). However, their long-term benefit is limited, as tumors develop acquired resistance over time (6). Several strategies have been tested to overcome resistance to anti-VEGF agents, including the use of agents targeting VEGF-independent pathways (bFGF, c-MET, IL8; refs. 7–9), or those responsible for hypoxia-induced tumor responses, such as mTOR (10). Unfortunately, these strategies have not significantly improved long-term outcomes in patients with tumors resistant to anti-VEGF agents (10–12). This constitutes a significant challenge in the field of cancer therapeutics, and underscores the urgent need to identify strategies that safely target novel pathways critical for tumor angiogenesis.

It appears that the glucose analogue, 2-deoxy-D-glucose (2-DG), provides such an opportunity. This agent inhibits glycolysis by competitive inhibition with phosphoglucose isomerase and allosteric interference with hexokinase. Because of its similarity to mannose, 2-DG is also known to interfere with N-linked glycosylation by competition with mannose metabolism and by fraudulent incorporation into dolichol-pyrophosphate (lipid)–linked oligosaccharides, which are the precursors of N-linked glycosylation (13, 14). We previously demonstrated that 2-DG significantly inhibits growth, migration, capillary formation, and induced apoptosis in growth factor–stimulated HUVECs (15), at lower concentrations (0.6 mmol/L) than those needed to induce tumor cell cytotoxicity (16–18). These effects were demonstrated to be due to 2-DG's interference with N-linked glycosylation, rather than glycolysis inhibition. *In vivo*, 2-DG inhibited neovessel formation in the Matrigel plug assay as well as tumor angiogenesis, in the $LH_{BETA}T_{AG}$ transgenic retinoblastoma model. In this report, we characterize the molecular mechanisms of endothelial sensitivity to 2-DG. The findings described below provide useful insight into novel mechanisms for angiogenesis inhibition.

Materials and Methods

Cell lines and reagents

2-DG, 2-FDG, oxamate, mannose, tunicamycin, and (2′Z, 3′E)-6-bromoindirubin-3′-oxime (BIO) were purchased from Sigma-Aldrich. Brefeldin A was acquired from Calbiochem-EMD

[1]Department of Medicine, Division of Hematology-Oncology, University of Miami Miller School of Medicine and Sylvester Comprehensive Cancer Center, Miami, Florida. [2]Bascom Palmer Eye Institute, Department of Ophthalmology, University of Miami Miller School of Medicine and Sylvester Comprehensive Cancer Center, Miami, Florida. [3]Department of Cell Biology, University of Miami Miller School of Medicine and Sylvester Comprehensive Cancer Center, Miami, Florida.

Note: Supplementary data for this article are available at Molecular Cancer Therapeutics Online (http://mct.aacrjournals.org/).

Current address for T.G. Murray: Murray Ocular Oncology and Retina, 6705 Red Road, Suite 412, Miami, FL 33143.

Corresponding Author: Jaime R. Merchan, University of Miami, 1475 NW 12th Avenue, Miami, FL 33136. Phone: 305-243-1287; Fax: 305-243-1293; E-mail: jmerchan2@med.miami.edu

doi: 10.1158/1535-7163.MCT-14-0315

Millipore. Matrigel was obtained from BD Biosciences and used at 7 mg/mL. Human bFGF and VEGF were purchased from R&D Systems. Human microvascular endothelial cells from lung (HMVEC-L) were purchased from Lonza in 2007, used only till passage 5 and was authenticated by vendor. EBM-2 basal medium and the EGM2 and EGM2-MV supplements were purchased from Lonza. Human umbilical vein endothelial cells (HUVEC, purchased 3–4 times yearly depending on usage and used till passage 5), human mammary adenocarcinoma cells (MDA-MB-231; purchased in 2007), and human colorectal adenocarcinoma cells (HT-29; purchased in 2012 and 2014) were purchased from the ATCC and were authenticated by vendor. For the endothelial cell experiments described below, "unstimulated endothelial cells" are defined as cells maintained with endothelial basal medium (EBM) with 1% FBS while "stimulated endothelial cells" are cells that were starved overnight (EBM and 1% FBS), and then treated with either bFGF or VEGF (10 ng/mL) the day of the experiment. Endothelial cell media contains 1 gm of glucose per liter (5.5 mmol/L).

2-DG uptake assay

HUVECs, human lung microvascular endothelial cells [HMVEC(L)], HT-29, and MDA-MB-231 cells were seeded in their appropriate media and conditions at 2×10^5 cells per well in 6-well plates. After incubation, medium was replaced with fresh "hot" medium (high-glucose DMEM with 300 μmol/L cold 2-DG and 1 μCi ^{3}H 2-DG, Perkin Elmer), and the sample was incubated for 5 or 30 minutes at 37°C and 5% CO_2. Medium was then removed, cells were rinsed three times (serum-free medium), and lysed with 0.5 mL of 1 N NaOH and a 10-second ultrasonication. A 0.25 mL sample was used for protein analysis. Radioactivity from the remaining sample was counted in a Packard CA2000 liquid scintillation spectrometer (Packard tri-carb 2900TR Liquid Scintillation Analyzer). Specific radioactivity was determined by dividing the total radioactivity applied to each sample by the total number of moles of hot 2-DG applied to each sample, as previously reported (17). Results are displayed as nmol/mg of protein (±SD), at 5 or 30 minutes.

Matrigel tube formation assay

The Matrigel tube formation was performed as previously described (15, 19, 20). For time course experiments, plates were incubated at 37°C in 5% CO_2, endothelial cell tube formation was assessed at 2, 4, 8, and 18 hours with an inverted photomicroscope (Nikon), and quantification of total tube length was performed as previously described. Experiments were done at least in duplicate and repeated at least twice.

Western blot analysis

Unstimulated or stimulated endothelial cells and serum (10%) stimulated tumor cells were treated with 2-DG or other agents, incubated for different time periods and lysed. Protein concentration was determined from lysates by the BCA assay (Thermo Scientific). Ten to 20 μg proteins were prepared with 4X Laemmeli sample buffer and separated in 10% or 4%–20% Mini-Protean TGX gel (Bio-Rad), transferred to 0.45 μm pore–sized polyvinylidene difluoride membranes (Bio-Rad) and probed (1:1,000 dilution) for AKT pSer^{473}, S6 pSer$^{240/244}$, ERK pThr^{202}/Tyr^{204}, GSK3β pSer^9, PERK pThr^{980}, cleaved caspase-3, cleaved-PARP, total-VEGFR2, VEGFR2 pTyr^{1175}, and PLC-γ1 pTyr^{783} (Cell Signaling Technology), GSK3β pTyr^{216} (Calbiochem), and GAPDH (1:20,000 dilution) for loading control (Rockland). After probing, membranes were processed as previously described (15, 18). Band intensities of replicate Western blot figures were quantified with ImageJ software, normalized to the corresponding GAPDH bands, and results presented as percentage of control (untreated cells) ± SEM.

Immunocytochemistry for total VEGFR2 in HUVECs

HUVECs were plated in starving medium in chamber slides (VWR) at 80,000 cells per chamber. The following day, cells were treated as indicated and incubated for 24 hours. After incubation, sections were washed with PBS and fixed with 4% paraformaldehyde at room temperature for 1 hour. Cells were then washed 3 times with PBS and blocked with 10% normal serum (goat) in 1% BSA + 0.1% TritonX-100 in PBS for 1 hour at room temperature. Sections were then probed with anti-totalVEGFR2 primary antibody (1:25; Abgent) and incubated overnight at 4°C. After two washes, Alexa Fluor 488 goat anti-rabbit IgG secondary antibody (Invitrogen) was applied (1:500; for 1 hour at room temperature). This was followed by three PBS washes; slides were mounted with anti-fade mounting medium (Molecular Probes) and analyzed by fluorescent microscopy. Representative pictures were taken with a Zeiss LSM700 confocal microscope at 63X.

N-glycan digestion

HUVECs were seeded on 10 cm dish (4×10^4) and treated with or without 0.6 mmol/L of 2-DG in endothelial cell growth medium, incubated for 24 hours, and lysed. Protein concentration was determined from lysates by the BCA assay (Thermo Scientific). Equal amounts of proteins (30 μg) were digested at 37°C in 300 mL reactions with sialidase (neuraminidase; specificity for a2-3, a2-6, and a2-8 N-acetyl-neuraminic acid residues), endo H (removes only high mannose and some hybrid types of *N*-linked carbohydrates), and PNGase F [removes almost all types of *N*-linked (Asn-linked) glycans: high mannose, hybrid, bi-, tri-, and tetra-antennary; New England BioLabs] according to the manufacturer's instructions. After 5-minute digestion with sialidase, or 40 minutes with endo H or PNGase F, digested and undigested samples were boiled with 4X Laemmeli sample buffer and analyzed with Western blot analysis for determination of VEGFR2.

In vivo studies

The $LH_{BETA}T_{AG}$ transgenic mouse model (21–23) was used to evaluate *in vivo* effects of periocular administration of 2-DG on tumor angiogenesis. Thirteen-week-old mice ($n = 7$ in first experiment and $n = 8$ in second experiment) were treated with either 2-DG (75 mg/kg or 1.5 mg in a 20 gm mouse) or balanced salt solution (vehicle control; Alcon Laboratories, Inc.). Each dose was administered in a total volume of 20 μL via subconjunctival injection in the right eye, twice a week for 2 or 3 weeks (separate experiments). Twenty-four hours after final treatment, mice were euthanized and eyes were enucleated for tumor studies.

Immunofluorescence staining for microvessel density

Measurement of tumor vasculature in retinoblastoma samples were performed as previously reported (15, 21), with minor modifications. Briefly, eyes were frozen in optimal cutting temperature (OCT) compound immediately following

Table 1. ^{3}H-2-DG uptake in HT-29 and MDA-MB-231 cancer cells and HUVEC and HMVEC(L)[a]

	Transport rate (nmol/mg protein ± SD)	
Cells	**5 minutes**	**30 minutes**
HT-29	5.2 ± 0.69[b]	21.4 ± 0.67[c]
MDA MB-231	4.1 ± 0.09	19.2 ± 0.91
HMVEC(L)	3.2 ± 0.21	14.9 ± 0.2
HUVEC	4.0 ± 0.26	19.7 ± 1.89

[a]See Materials and Methods section for description of experiments.
[b]$P = 0.0086$, HT-29 versus HUVEC; $P = 0.0005$, HT-29 versus HMVEC.
[c]$P = 0.002$ HT-29 versus HMVEC.

enucleation and serially sectioned (8 μm). Slides were fixed with methanol for 10 minutes (−20°C) before immunohistochemical analyses. Total vessels were detected with biotin-labeled lectin (*Bandeira simplicifolia*, a pan endothelial binding agent; 1:1,000, Sigma) and Cy3-conjugated streptavidin (1:500; Sigma). Neovessels were detected with α-endoglin (1:1,000; Santa Cruz Biotechnology) and Alexa Fluor 488–conjugated α-IgG2 (1:500, Invitrogen). Omission of the primary antibody (secondary only) was used as a negative control for nonspecific binding. Cell nuclei were stained for 5 minutes with 4′, 6′ diamidino-2-phenylindole (1:5,000; Invitrogen). All tumor areas were digitally imaged at 200X magnification with appropriate fluorescent filters on an Olympus BX51 microscope. Fluorescent signal intensities were analyzed separately, and then merged using Photoshop CS (Adobe). Differences in intraocular tumor vasculature between control and treated animals were measured by thorough quantification (in arbitrary units) of lectin or endoglin fluorescence signals within the total tumor area (vessel/tumor ratio) from all micrographs. Tumor vascular densities were displayed as mean percentages of total tumor areas ± SEM.

In vivo assessment of tumor unfolded protein response and apoptosis

Tumor samples were processed as above, and 8 μm frozen tumor sections were washed with PBS and fixed with 4% paraformaldehyde at room temperature for 1 hour. For determination of tumor unfolded protein response (UPR), sections were fixed as above and slides were washed 3 times and blocked with 10% normal serum (goat) in 1% BSA + 0.1% TritonX-100 in PBS for 1 hour at room temperature. Sections then were costained with anti-CD105–conjugated w/Alexa Fluor 488 (endoglin for angiogenic endothelial cells; dilution 1:50) and anti GRP78 (BiP) antibody (dilution 1:100; Cell Signaling Technology) for URP and incubated overnight in the cold room. This was followed by washes and then incubation with the secondary antibody Alexa Fluor 647 (Invitrogen; 1:500 dilution). This was followed by three PBS washes and slides were treated with anti-fade mounting medium

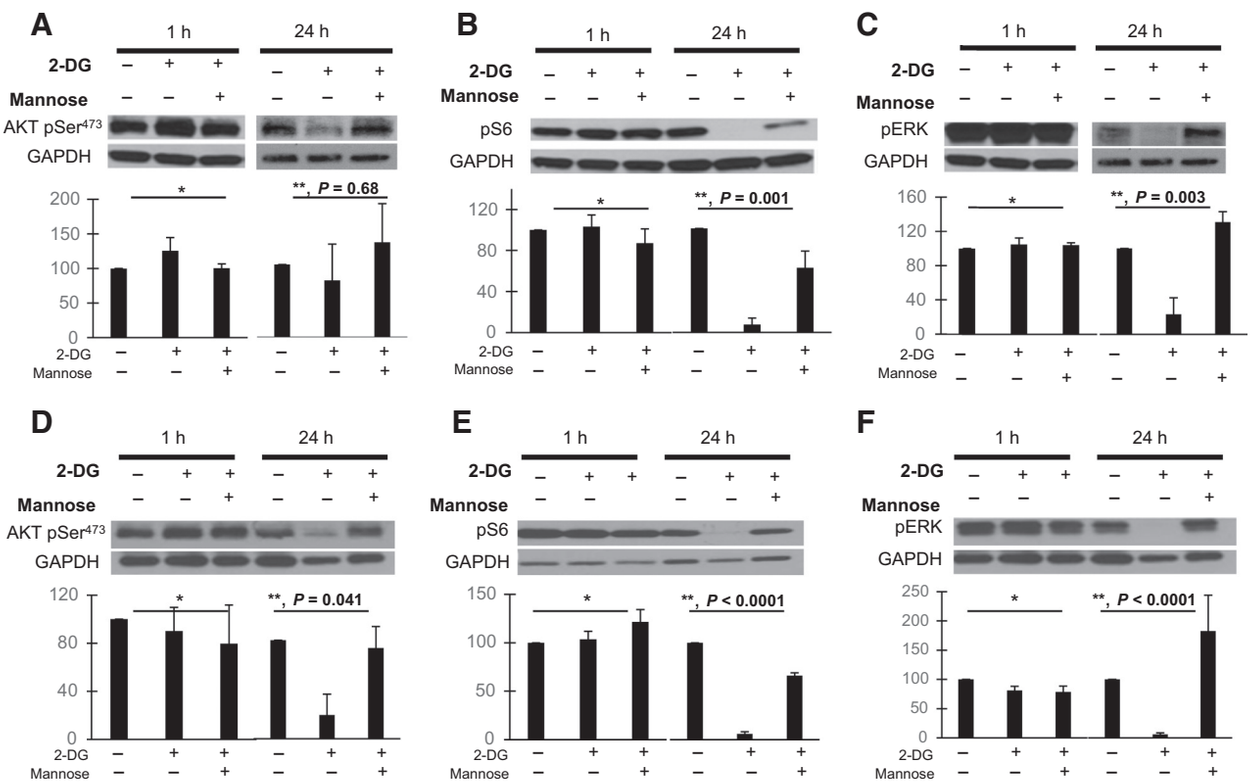

Figure 1.
Effects of low-dose 2-DG on endothelial PI3K/mTOR and ERK pathways *in vitro*. Starved HUVECs were stimulated with VEGF (A–C) or bFGF (D–F), treated with 0.6 mmol/L 2-DG ± 1 mmol/L mannose, and incubated for 1 or 24 hours. Lysates were used in standard Western blot procedure (Materials and Methods). Membranes were then blotted against AKT pSer^{473}, S6 pSer$^{240/244}$, ERK pThr^{202}/Tyr^{204}, and GAPDH as loading control. Band intensity was analyzed by densitometry, normalized to GAPDH, and results displayed as means (±SEM) of relative protein density (percent) compared with untreated controls. GAPDH bands from A, C, D, and F are similar as phosphoproteins were blotted from the same membranes. *, *P* value not significant; **, untreated versus 2-DG–treated growth factor–stimulated HUVECs. Pictures are representative of experiments performed at least in triplicate.

(Molecular Probes) and analyzed for apoptotic endothelial cells by fluorescent microscopy. Representative pictures were taken with a Zeiss LSM700 confocal microscope at 40X.

To detect and visualize apoptosis, slides were washed twice with PBS (after fixation), permeabilized with 0.2% TritonX-100 for 20 minutes at room temperature and after 2 additional washes with PBS, sections were probed with label solution (for negative controls) or TUNEL reaction mix, following manufacturer's instructions (*In Situ* Cell Death Detection Kit; Roche Applied Science). Sections then were probed with anti-CD31 antibody (eBioscience; 1:50 dilution) and incubated overnight at 4°C. After 2 washes, Alexa Fluor (Red) 555 goat anti-rat IgG(H+L) (Invitrogen) secondary antibody was applied at a 1:500 dilution for 1 hour at room temperature. Then slides were washed, mounted, and analyzed with confocal microscope as described above.

Laser capture microdissection of tumor tissues

Tumor tissue was isolated from sections obtained from the above experiments. Eight micron sections were placed onto Director Laser Microdissection slides (Expression Pathology) and stained with hematoxylin. Areas containing tumor cell nuclei were microdissected, using a Leica AS LMD laser microdissection system. Approximately 50,000 tumor cells were dissected from each section and collected into Eppendorf caps containing 50 μL of Lysis Buffer with β-mercaptoethanol. GRP78 expression was determined by immunoblot of LCM protein samples. Protein isolation and immunoblot from LCM samples was performed as described (24).

Statistical analysis

Data are presented as means ± SEM (*in vitro* experiments) or SEM (*in vivo* experiments). Differences in means among three or more groups were analyzed by ANOVA. Pairwise comparisons were performed using the Tukey–Kramer method. Means between two groups were compared by Student *t* test analysis. Differences were considered statistically significant at $P < 0.05$.

Results

Comparative analysis of 2-DG transport in endothelial and tumor cells

Human endothelial cells (HUVEC, HMVEC) are significantly more sensitive to the cytotoxic effects of 2-DG compared with tumor cells (15). To test the hypothesis that differences in sensitivity to low doses of 2-DG between endothelial and cancer cells are due to differential drug transport, cellular uptake of radioactive 2-DG was measured. Drug transport was

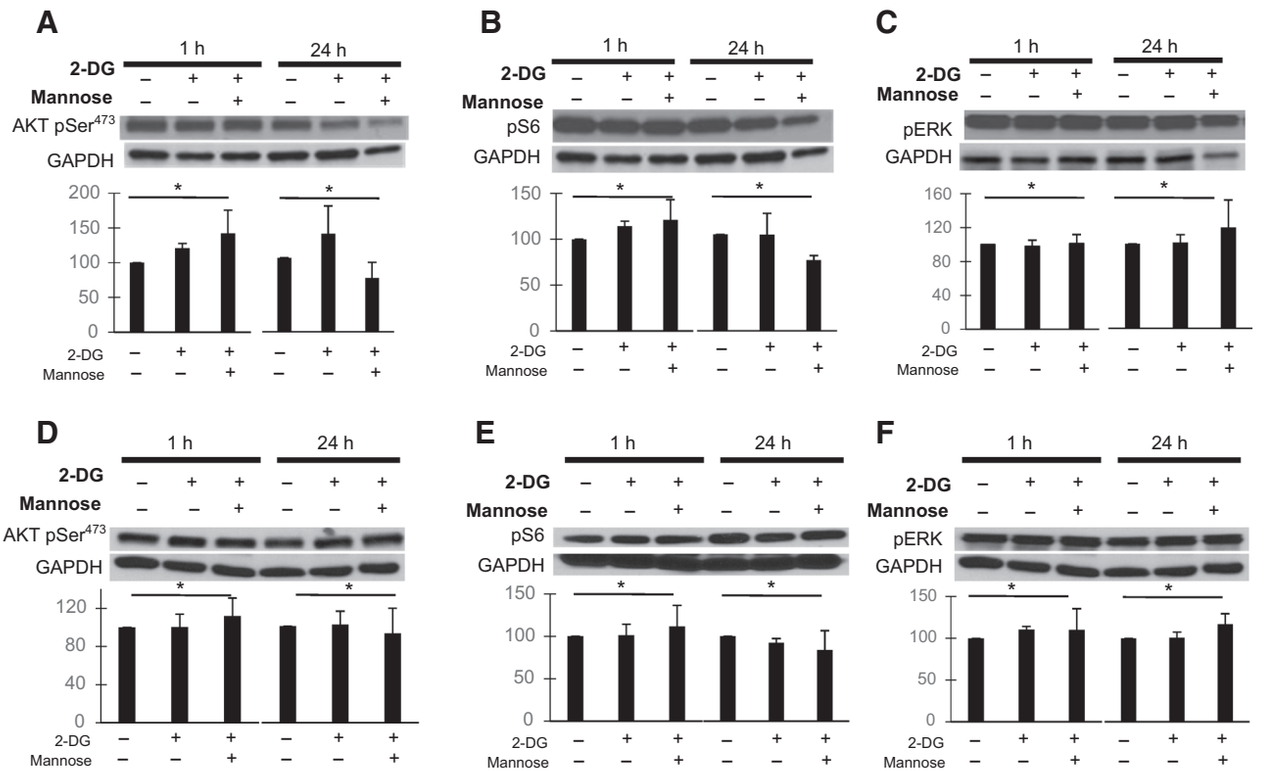

Figure 2.
Effects of low-dose 2-DG on tumor cell PI3K/mTOR and ERK pathways *in vitro*. MDA-MB-231 (A–C) and HT-29 (D–F) cancer cell lines were stimulated with 10% serum, treated with 0.6 mmol/L 2-DG ± 1 mmol/L mannose, and incubated for 1 or 24 hours. Lysates were used in standard Western blot procedure (Materials and Methods). Membranes were then blotted against AKT pSer^{473}, S6 pSer$^{240/244}$, ERK pThr^{202}/Tyr^{204}, and GAPDH as loading control. Band intensity was analyzed by densitometry, normalized to GAPDH, and results displayed as means (±SEM) of relative protein density (percent) compared with untreated controls. GAPDH bands from A, B, D, and F are similar, as the corresponding phosphoproteins were blotted from the same membranes. *, *P* value not significant. Pictures are representative of experiments performed at least in triplicate.

not increased in endothelial cells compared with cancer cells, at 5 or 30 minutes (Table 1). HT-29 cells had significantly higher drug uptake compared with HUVEC ($P = 0.0086$) and HMVEC ($P = 0.0005$) at 5 minutes and compared with HMVEC at 30 minutes ($P = 0.0002$). VEGF or bFGF stimulation modestly (but not significantly) increased 2-DG transport in HUVECs at 1 hour, but not a 24 hours, compared with controls (Supplementary Table S1). Growth factor stimulation did not increase 2-DG uptake in HMVECs.

Differential effects of 2-DG on endothelial versus tumor cell AKT, mTOR, and ERK phosphorylation

Endothelial proliferation, capillary formation, migration, and survival (all affected by 2-DG; ref. 15) are regulated in part by the PI3K/AKT and MAPK pathways (25–27); therefore, we investigated the effects of low-dose 2-DG on these pathways in endothelial cells and tumor cells. While no significant effects were observed in HUVECs when treated with 2-DG at 1 hour, at 24 hours, AKT_{473} (Fig. 1A and D), S6 (Fig. 1B and E), and ERK phosphorylation (Fig. 1C and F) were significantly downregulated, and the effects were reversed by cotreatment with mannose. The effects of 2-DG on AKT phosphorylation were more marked in HUVECs treated with bFGF (Fig. 1D) than with VEGF (Fig. 1A), while pS6 (Fig. 1B and E) and pERK (Fig. 1C and F) downregulation were equally potent in HUVECs stimulated with either growth factor. In contrast, downregulation of these pathways was not observed in MDA-MB-231 (Fig. 2A–C) or HT-29 (Fig. 2D–F) cancer cell lines when similarly treated. ERK and S6 were found to be significantly downregulated by 2-DG at 8 hours in HUVECs exposed to either VEGF or bFGF, whereas AKT was mildly increased (Fig. 3A–C).

Effects of other glycolytic inhibitors on endothelial AKT and ERK pathways

The finding that 2-DG's inhibition of AKT and ERK is reversible by mannose strongly suggests that these effects depend on 2-DG's interference with endothelial N-linked glycosylation, and not glycolysis. To further support this interpretation, the effects of equimolar concentrations (0.6 mmol/L) of fluoro-deoxygluose (FDG, a more potent glycolytic inhibitor and weaker N-glycosylation inhibitor than 2-DG), and oxamate (a glycolytic inhibitor with no detectable ER stress-inducing activity) on the above pathways were investigated. Neither FDG nor oxamate had effects on AKT or ERK phosphorylation

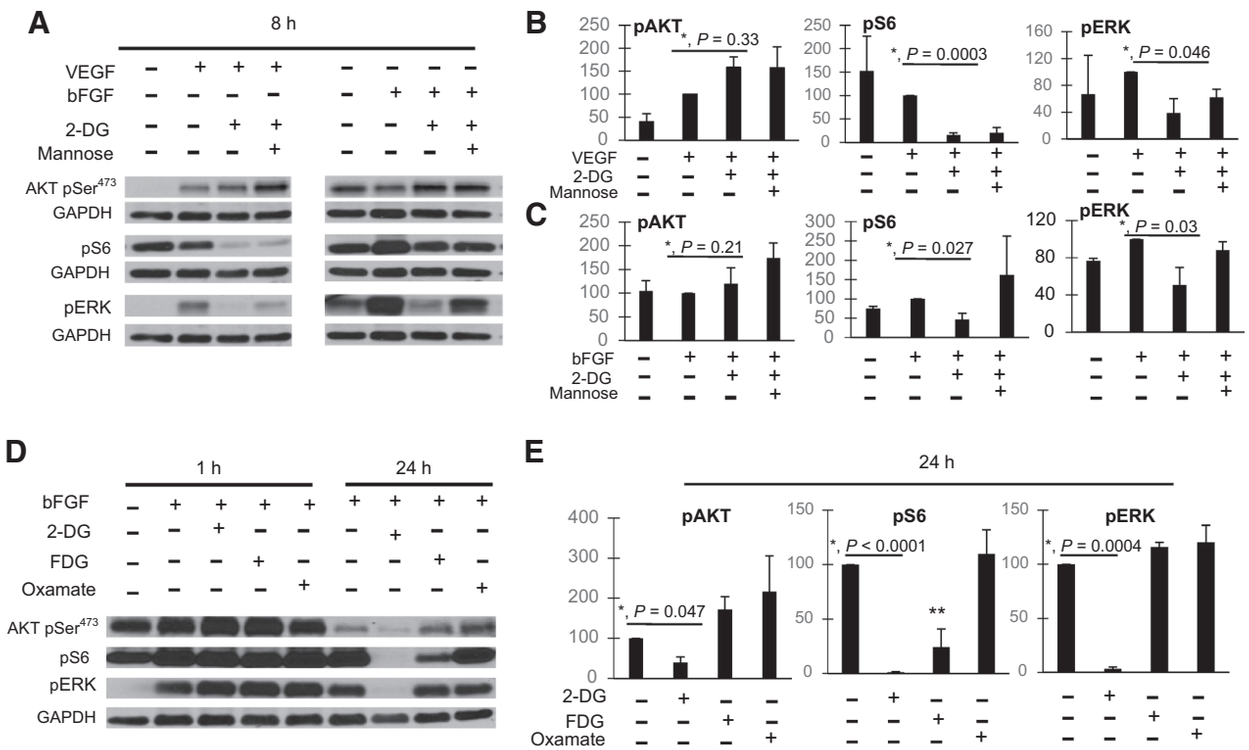

Figure 3.
Effects of 2-DG and other glycolytic inhibitors on endothelial AKT/mTOR and ERK. A, growth factor (VEGF, bFGF)-stimulated HUVECs were treated with 0.6 mmol/L 2-DG with or without 1 mmol/L mannose and incubated for 8 hours. Lysates were used for Western blot determination of AKT $pSer^{473}$, S6 $pSer^{240/244}$, ERK $pThr^{202}/Tyr^{204}$, and GAPDH as loading control. Band intensity was analyzed by densitometry, normalized to GAPDH, and results displayed as means (±SEM) of relative protein density (percent) compared with untreated controls. GAPDH bands corresponding to AKT pSer473 and pERK are the same, as phosphoproteins were blotted from the same membrane. Densitometry data are presented from HUVECs exposed to VEGF (B) or bFGF (C). *, untreated versus 2-DG–treated growth factor–stimulated HUVECs. D, bFGF-stimulated HUVECs were treated with 0.6 mmol/L 2-DG, FDG, or oxamate and incubated for 1 or 24 hours and levels of AKT $pSer^{473}$, S6 $pSer^{240/244}$, and ERK $pThr^{202}/Tyr^{204}$ were assessed by Western blot analysis. GAPDH loading control is the same for 3 phosphoproteins, as they were blotted from the same membrane. E, densitometry data are presented from HUVECs at 24 hours after treatment with 2-DG. *, untreated versus 2-DG–treated growth factor–stimulated HUVEC; **, $P = 0.046$, FDG versus. control.

(Fig. 3D and E) whereas FDG, but not oxamate, decreased S6 phosphorylation, albeit to a lower degree compared with 2-DG.

Correlation between the dynamics of ERK downregulation by 2-DG and inhibition of endothelial tube formation

Endothelial capillary formation, disrupted by 2-DG, is a dynamic process that is regulated in part by ERK (25, 27). To determine whether the timing of endothelial ERK inhibition correlated with the effects of 2-DG on tube formation, 2-DG–treated HUVECs were plated on Matrigel and tube formation was observed at 2, 4, 8, and 18 hours. Clear inhibition of endothelial tube formation was observed at 8 hours of treatment, compared with controls, and the effects were more marked at 18 hours (Fig. 4).

Effects of 2-DG on endothelial VEGFR2

The VEGF promotes angiogenesis by binding to its endothelial receptors, mainly VEGFR2, with subsequent activation of downstream signaling (28, 29). As VEGFR2 undergoes posttranslational N-linked glycosylation (28), we investigated the influence of 2-DG on this receptor.

In HUVECs simultaneously treated with 2-DG, we observed changes in the migration pattern of total VEGFR2 compared with untreated cells. While control cells showed a normal, mature VEGFR2 (migrating at 210–230 kDa), in 2-DG–treated cells, VEGFR2 migrated at a lower molecular size (approximately 150 kDA, Fig. 5A), consistent with the production of unglycosylated, immature VEGFR2 (28). The observed effects were mannose reversible.

To further investigate whether the shift of VEGFR2 migration induced by 2-DG was due to VEGFR2 hypoglycosylation, we performed selective digestion of HUVEC lysates treated with 2-DG or controls, using N-glycan–digesting enzymes (sialidase, endo-H) as well as PNGase F (see Materials and Methods), and Western blot analysis for VEGFR2 was performed. We observed a clear difference in the VEGFR2 digestion patters between control and 2-DG–treated cells (Fig. 5B). Control (untreated) samples were sensitive to sialidase (mild decrease in receptor migration, due to removal of terminal sialic acid residues). While the upper VEGR2 band was sensitive to this enzyme as well as PNGase F, the lower band was cleaved by both endoH and PNGase F. On the other hand, VEGFR2 from HUVECs treated with 2-DG were resistant to sialidase treatment and had a similar digestion pattern after both endo H and PNGase F digestion (we observed the presence of intermediate bands in control, but not 2-DG–treated cells after digestion with endo H and PNGase F. The significance of those bands is not clear, but may represent partially digested VEGFR2 in the control cells).

To further confirm that changes in VEGFR2 migration pattern were due to interference with N-linked glycosylation, we examined the effects of tunicamycin, an inhibitor of N-linked glycosylation, and Brefeldin A (BFA), an agent that induces ER stress without inhibiting N-linked glycosylation (30). While the glycosylation inhibitors 2-DG and tunicamycin had similar effects on VEGFR2 migration, BFA did not (Fig. 5C).

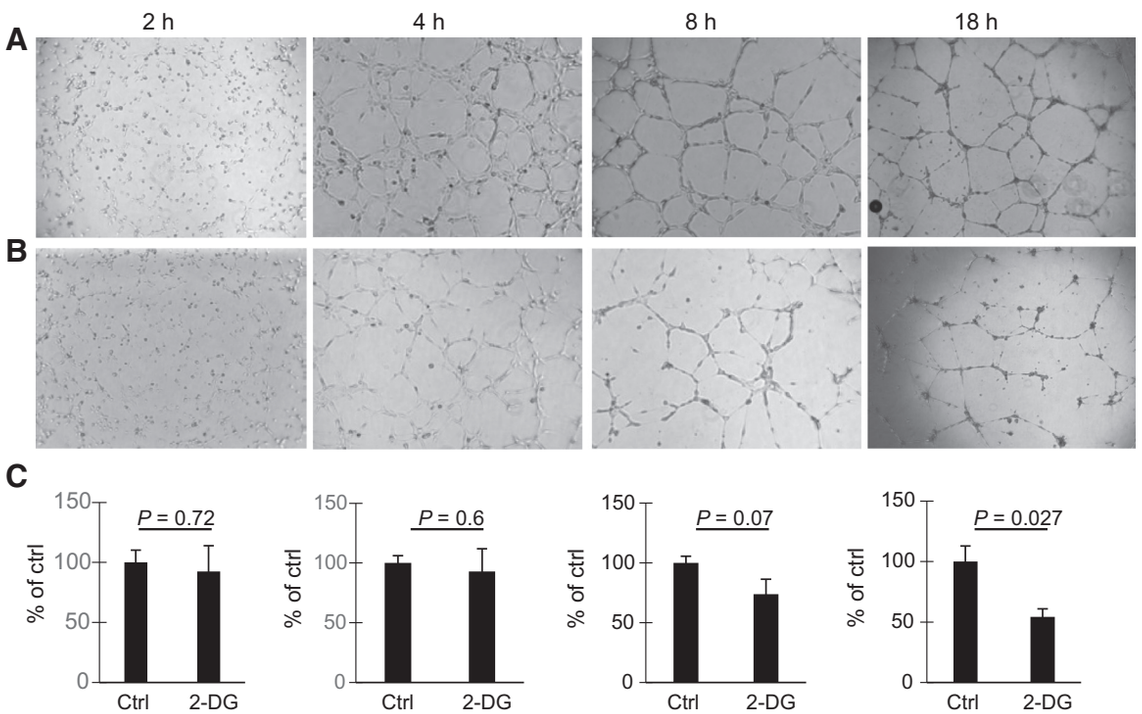

Figure 4.
Effects of 2-DG on HUVEC tube formation. HUVECs were plated in Matrigel-coated wells and treated with PBS (A) or 0.6 mmol/L 2-DG (B). Tube formation was assessed and photographed at 2, 4, 8, and 18 hours. Scale bar, 500 μm. C, quantitative analysis of total tube length was performed as described in Materials and Methods. Histograms represent the average (±SEM) tube length (percent of control) of duplicate experiments, repeated at least twice.

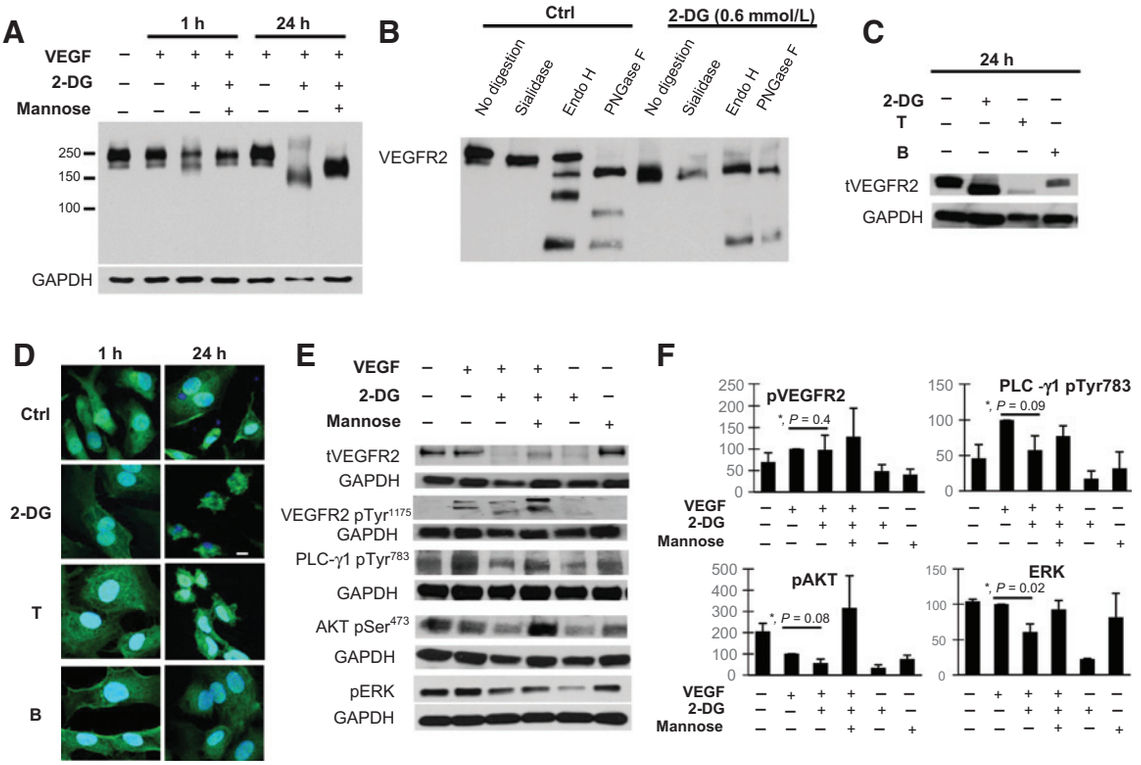

Figure 5.
Effects of 2-DG on endothelial VEGFR2. A, HUVECs were stimulated with VEGF and treated with 0.6 mmol/L 2-DG with or without 1 mmol/L mannose for 1 or 24 hours. Total VEGFR2 was demonstrated by Western blot analysis, using a low percentage gel to show the complete migration pattern. B, HUVECs were treated with vehicle or 2-DG for 24 hours, and lysates digested with sialidase, endo H, or PNGase F, as described in Materials and Methods. Western blot analysis for total VEGFR2 was performed from digested samples. C, HUVECs were stimulated as above and treated with 2-DG, tunicamycin (T, 0.25 μg/mL) or Brefeldin A (BFA, 50 nmol/L). Western blot determination of total-VEGFR2 and GAPDH was performed from cell lysates at 24 hours of treatment. D, endothelial VEGFR2 expression was assessed by immunofluorescence staining. VEGF-stimulated HUVECs were treated with 2-DG, tunicamycin, or Brefeldin as above. Pictures are representative of triplicate experiments. Scale bar, 10 μm. E, HUVECs in starving medium were treated with 0.6 mmol/L 2-DG (±1 mmol/L Mannose) for 24 hours, then stimulated with VEGF for 1 hour. Total and phosphor-VEGFR2 (VEGFR2 Tyr^{1175}), activated PLC-γ1 (PLC-γ1 $pTyr^{783}$), AKT (AKT $pSer^{473}$), and ERK (ERK $pThr^{202}/Tyr^{204}$) were assessed by Western blot analysis of cell lysates. F, band intensity was analyzed by densitometry, normalized to GAPDH, and results displayed as means (±SEM) of relative protein density (percent) compared with untreated controls. *, untreated versus 2-DG–treated growth factor–stimulated HUVECs.

Immunofluorescent determination of VEGFR2 demonstrated that receptor expression is not inhibited after 2-DG treatment either at 1 or 24 hours after treatment (Fig. 5D). Even though HUVECs exposed to 2-DG (or the N-linked glycosylation inhibitor tunicamycin) for 24 hours displayed significant changes in cell size and shape (due to apoptosis induced by the drug), receptor expression was observed. The above findings indicate that 2-DG, while not significantly affecting expression, interferes with VEGFR2 N-linked glycosylation, leading to an immature, lower molecular weight isoform.

To further investigate the functional consequences of 2-DG–induced changes on VEGFR2, the above treatment conditions were modified: HUVECs were pretreated with 2-DG for 24 hours, before stimulation by VEGF, and immunoblots of pVEGFR2, and downstream signaling mediators were performed 1 hour after stimulation. Under these conditions, 2-DG decreased the levels of total VEGFR2, as expected. Even though phosphorylation of the smaller molecular size VEGFR band was observed, activation of its downstream adaptor PLC-γ1 $pTyr^{783}$ was decreased and AKT and ERK were downregulated as compared with the control cells (Fig. 5E and F). These effects were attenuated by cotreatment with mannose further indicating that they were due to 2-DG interfering with N-linked glycosylation.

Role of GSK3β on 2-DG–mediated endothelial apoptosis and pathway inhibition

We have previously shown that 2-DG induces endothelial N-linked glycosylation, leading to induction of ER stress and apoptosis (15). As GSK3β plays a critical role in ER stress–mediated apoptosis (31–33), and reports suggest its involvement in AKT and ERK regulation (34, 35) in tumor cells, we investigated the role of GSK3β on 2-DG–mediated endothelial apoptosis. At 24 hours, 2-DG induced ER stress in HUVECs, as demonstrated by increased levels of phosphorylated PERK and its downstream eIF2α (Fig. 6). Moreover, 2-DG induced GSK3β activation, as shown by decreased levels of the inhibitory GSK3β $pSer^{9}$ (refs. 35, 36; Fig. 6) and were associated with apoptosis, as shown by increased levels of cleaved caspase-3 and cleaved PARP in treated endothelial cells. These effects occurred in HUVECs exposed to either VEGF (Fig. 6A and B) or bFGF (Fig. 6C and D) and were reversed by mannose.

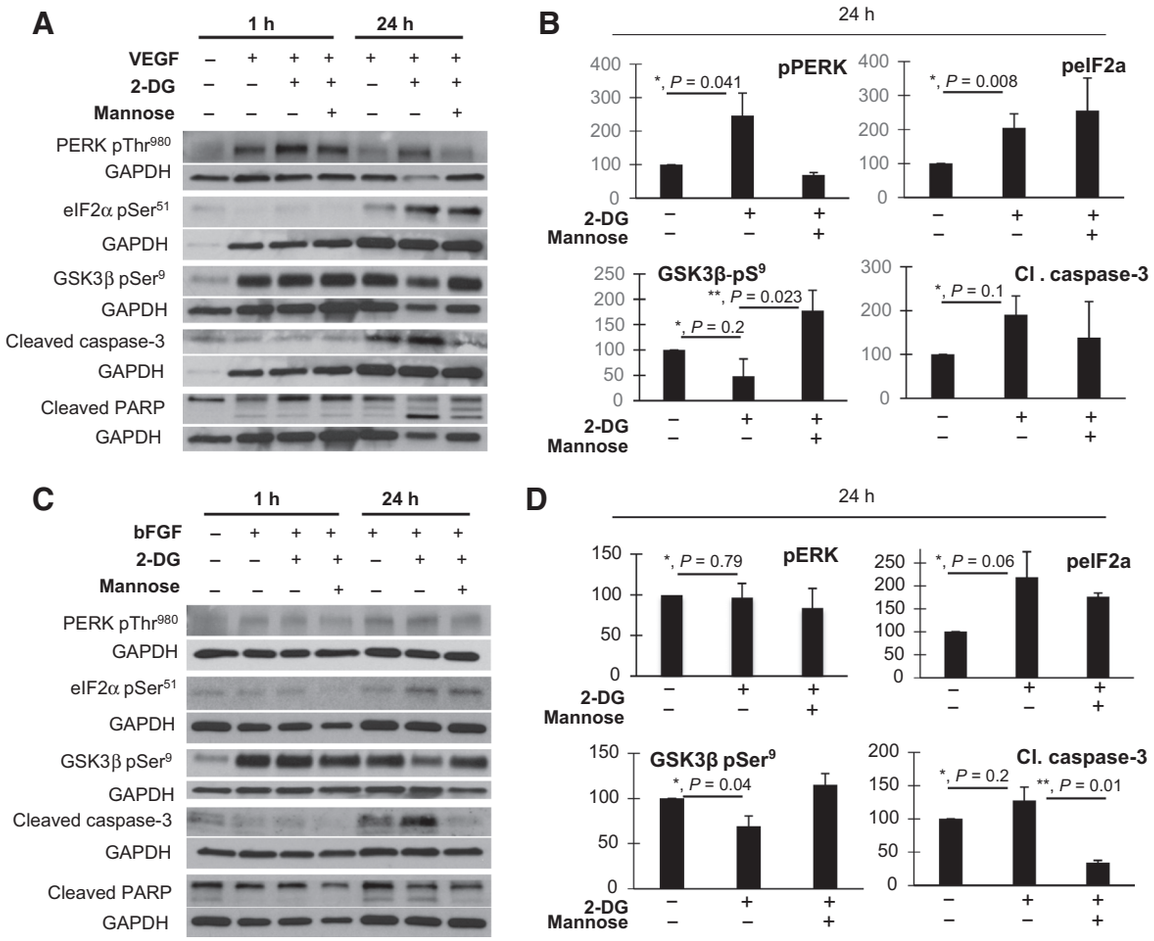

Figure 6.
Effects of 2-DG on endothelial endoplasmic reticulum (ER) stress, GSK3β, and apoptosis. A–D, growth factor–stimulated HUVECs (A and B, VEGF; C and D, bFGF) were treated with 2-DG as described and endothelial ER stress was assessed by activated PERK (PERK pThr^{980}) and eIF2α (eIF2α pSer^{51}). GSK3β activation status was evaluated by determination of GSK3β pSer^{9} (inhibitory site) levels. Cleaved caspase-3 (Cl caspase-3) and cleaved PARP were assessed to determine apoptosis. Band intensity from 24-hour samples was analyzed by densitometry, normalized to GAPDH, and results displayed as means (±SEM) of relative protein density (percent) compared with untreated controls. A–C, GAPDH bands corresponding to GSK3β and cleaved PARP, eIF2α and cleaved caspase-3 (A), and those corresponding to eIF2α and cleaved PARP (C) are similar, as phosphoproteins were blotted from the same corresponding membranes (for VEGF- or bFGF-stimulated cells). *, untreated versus 2-DG–treated growth factor–stimulated HUVECs. **, 2-DG versus 2-DG + mannose-treated, growth factor–stimulated HUVECs.

Next, HUVECs were treated with 2-DG in the presence or absence of the GSK3β inhibitor bromoindirubin-3′-oxime (BIO). As shown in Fig. 7, under these conditions, 2-DG–induced apoptosis was blocked. In addition, BIO partially reversed 2-DG–induced ERK downregulation, but did not reverse AKT inhibition. These effects occurred regardless of bFGF (Fig. 7A and B) or VEGF (Fig. A, C) exposure to HUVECs.

2-DG inhibits tumor neovessels, induces ER stress and apoptosis *in vivo*

We previously showed that 2-DG inhibits angiogenesis *in vivo*, in the Matrigel plug assay and in the $LH_{BETA}T_{AG}$ mouse model of retinoblastoma (15). To further characterize the *in vivo* antiangiogenic effects of 2-DG, $LH_{BETA}T_{AG}$ mice were treated with periocular injections of 2-DG twice a week for 2 weeks as described in Materials and Methods. In addition to its effects on total (lectin^{+}) tumor vasculature, 2-DG–treated mice had a significant reduction of newly formed (endoglin^{+}) microvessels ($P = 0.0032$), compared with controls (Fig. 8A and B). Repeat experiments, where mice were treated for a period of 3 weeks, showed predominant effects on endoglin-positive neovessels, compared with total vessels (Supplementary Fig. S1).

Moreover, tumors of 2-DG–treated (but not control) animals demonstrated increased tumor UPR response, as detected by positive GRP78 immunofluorescence (Fig. 8C and Supplementary Fig. S2) and immunoblot determination of tumor tissue extracted by laser capture microdissection (Supplementary Fig. S3). GRP78–positive areas in the 2-DG–treated tumors showed costaining with CD105 (endoglin, arrows in Fig. 8C). To assess for *in vivo* apoptosis, the terminal deoxynucleotidyl transferase–mediated dUTP nick end labeling (TUNEL) assay

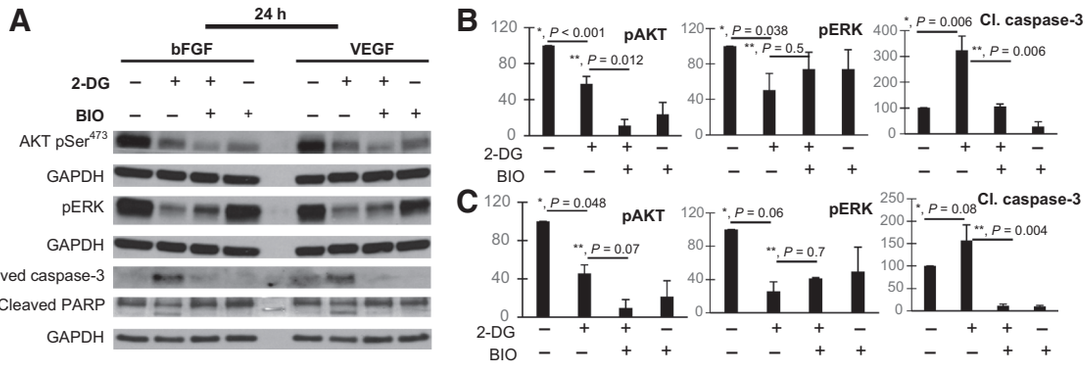

Figure 7.
Effects of GSK3β inhibition on 2-DG induced endothelial AKT/ERK downregulation and apoptosis. Growth factor–stimulated HUVECs were treated with 0.6 mmol/L 2-DG with or without the GSK3β inhibitor BIO (5 nmol/L), for 24 hours. Lysates were processed and AKT pSer^{473} and ERK pThr^{202}/Tyr^{204}, cleaved caspase-3, and cleaved PARP were demonstrated using standard Western blot procedures (A). Densitometry analysis of bFGF (B)- and VEGF (C)-exposed HUVECs. GAPDH bands corresponding to pAKT and pERK (for each growth factor) are similar, as phosphoproteins were blotted from the same membrane. *, untreated versus 2-DG–treated growth factor–stimulated HUVECs; **, 2-DG versus 2-DG + BIO-treated, growth factor–stimulated HUVECs.

was performed, along with CD31 costaining. Tumors from animals treated with 2-DG showed increased TUNEL-positive areas, compared with control tumors (Fig. 8D). In addition, colocalization of TUNEL-positive and CD31-positive areas was frequently found in treated tumors, compared with control tumors (arrows in Fig. 8D).

Discussion

When switching from quiescence to angiogenesis, endothelial cells have the ability to adapt their metabolism, allowing them to sustain cell growth and capillary formation in hypoxic microenvironments, in a manner similar to tumor cells (30, 37, 38). This adaptation provides an opportunity to exploit tumor as well as endothelial metabolism for therapeutic gain. 2-DG, which is currently undergoing preclinical and early clinical development for cancer treatment (39–41) inhibits angiogenesis at concentrations significantly lower than those required for tumor cell cytotoxicity (15). In this report, we found that endothelial cell hypersensitivity cannot be merely explained on differential uptake as tumor cells were found to accumulate as much or more radiolabeled 2-DG. Rather, we found that endothelial cell sensitivity to this agent was associated with endothelial-selective downregulation of AKT and ERK (Figs. 1 and 2). These effects were reversible by mannose, and did not occur with oxamate or 2-FDG, indicating that ERK and AKT downregulation is a result of 2-DG's interference with N-linked glycosylation and not glycolysis. Importantly, they were independent of the type of growth factor

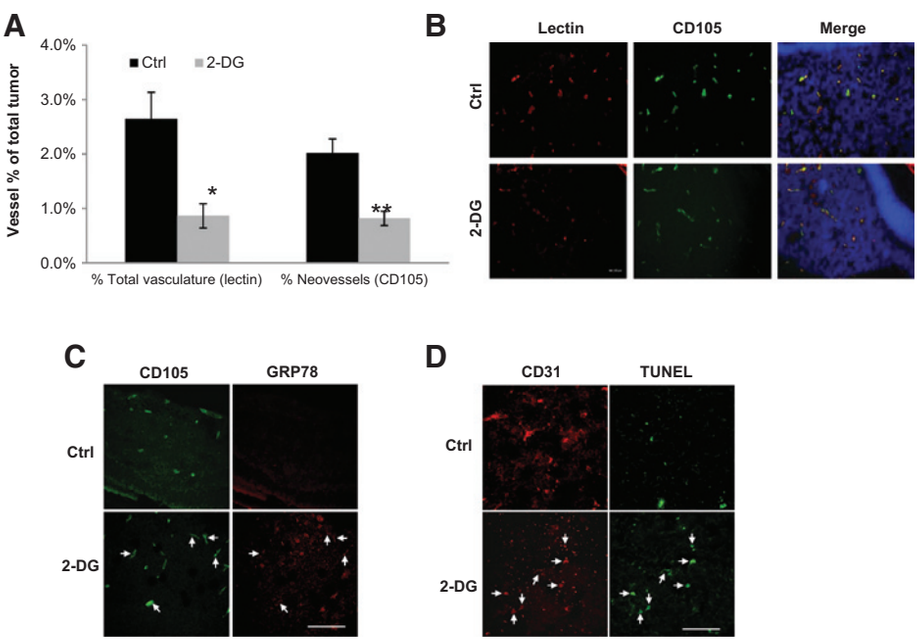

Figure 8.
In vivo effects of 2-DG on tumor angiogenesis and induction of UPR, and apoptosis. $LH_{BETA}T_{AG}$ mice were treated with 2-DG or vehicle as described in methods. A, quantification of tumor microvessel density (total vasculature and neovessels) is presented as percent of total tumor area. Bars, means ± SEM of at least four independent samples per group. *, $P = 0.0079$; **, $P = 0.0032$, respectively. B, representative pictures of total and neovessels in control and 2-DG–treated samples. C, tumor samples were stained for GRP78 and CD105 (endoglin). Arrows represent CD105- and GRP78-positive areas. D, in this experiment, mice were treated for 3 weeks as in methods. Samples were stained for apoptosis (TUNEL) and tumor endothelium (CD31). Representative pictures of experiments performed in quadruplicate. Arrows represent CD31 and TUNEL-positive microvessels. Scale bars, 100 μm.

used to stimulate endothelial cells (i.e., FGF or VEGF) and not observed in the tumor cells tested.

The kinetics of ERK and AKT downregulation were found to be different and correlated with specific biologic effects of 2-DG on endothelial cells. ERK (but not AKT) downregulation was observed as early as 8 hours after 2-DG treatment (Fig. 3A), an effect that coincided with inhibition of tube formation, also detected as this time point. Conversely, AKT inhibition was not seen until 24 hours of treatment, which is the time we previously reported that endothelial cells undergo apoptosis when treated with 2-DG (15). These results suggest that 2-DG–induced downregulation of ERK as opposed to AKT may play a more critical role in interfering with tube formation and perhaps with subsequent cell death. Our findings are in agreement with prior reports showing that silencing ERK with siRNA blocks tube formation, induces cell death *in vitro*, and suppresses angiogenesis *in vivo* (25, 42, 43). A previous report has shown that high concentrations (25 mmol/L) of 2-DG were found to increase AKT and ERK activation in multiple cancer cell lines (44). These marked differences in endothelial versus tumor cell regulation of ERK and AKT by 2-DG may therefore explain the increased endothelial sensitivity to this sugar analogue.

Our data indicate that 2-DG's interference with endothelial N-linked glycosylation leads to VEGF receptor hypoglycosylation as well as to induction of ER stress, either of which can result in downregulation of ERK and AKT. It is important to emphasize that 2-DG did not reduce VEGFR2 expression, but rather induced receptor hypoglycosylation, as demonstrated by changes in VEGFR2 migration, as well as differential VEGFR2 digestion pattern after treatment with sialidase, endo H, and PNGase F. These effects lead to decreased downstream signaling, as shown by lower levels of phosphorylated PLC-γ1, AKT, and ERK. The findings that mannose reversed 2-DG's effects on VEGFR2 migration and downstream signaling, and that tunicamycin also induced similar changes in receptor migration patterns confirm that the changes were indeed due to interference with N-linked glycosylation. Our observations are in agreement with those of Nacev and colleagues, who found that the antifungal agent itraconazole interfered with VEGFR2 glycosylation, altered receptor trafficking, and decreased cell surface expression and downstream signaling (45). As many endothelial and cell surface receptors involved in anti-VEGF resistance mechanisms, such as EGFR, bFGF, cMET (45–48) are heavily glycosylated, our results suggest that agents that disrupt N-linked glycosylation, such as 2-DG, may prove useful in overcoming resistance to current clinically available anti-VEGF agents.

A key observation in this report was the finding that induction of ER stress by low concentrations of 2-DG leads to endothelial apoptosis via activation of GSK3β. The role of GSK3β in 2-DG–induced apoptosis was confirmed by the results with an inhibitor of this kinase, BIO, which reversed 2-DG–induced endothelial caspase-3 and PARP cleavage (Fig. 7). This, and the observation that BIO partially reverses 2-DG–induced ERK downregulation, suggests that GSK3β is involved in 2-DG's antiendothelial effects related to ER stress induction. Our findings are in agreement with a report by Kim and colleagues, which showed that expression of a constitutively active mutant of GSK3β induces endothelial apoptosis (49).

The mechanism of GSK3β activation by ER stress signals is thought to involve dephosphorylation, by protein phosphatase 2A, of the (inhibitory) phospho-Ser-9 of the kinase (32). The same mechanism may mediate ER stress induced AKT 473 dephosphorylation, an effect shown in neuronal cells upon induction of ER stress by thapsigargin (32). Meares and colleagues showed that GSK3β activation mediates ER stress induced apoptosis by activation of the death inducing transcription factor C/EBP homologous protein (CHOP/GADD153) (33). Taken together, our findings indicate that activation of endothelial GSK3β by low-dose 2-DG may represent a novel and attractive antiangiogenic strategy.

The *in vivo* relevance of the above findings was demonstrated in the $LH_{BETA}T_{AG}$ retinoblastoma model, by showing that 2-DG induces the UPR *in vivo*, inhibits not only total, but especially newly formed ($CD105^{+}$) tumor microvessels, and induces endothelial apoptosis in a tumor animal model. This further validates the previous reports by us and others showing that inhibitors of N-linked glycosylation are associated with antiangiogenic and antitumor effects (15, 50). While this study validates the induction of *in vivo* ER stress and apoptosis after 2-DG treatment, the role of VEGFR2 hypoglycosylation on the *in vivo* effects is not known. Studies to further characterize the effects of 2-DG on VEGFR2 glycosylation and downstream signaling on *in vivo* tumor models are underway.

The translational implications of our data are multiple: First, the observation that AKT and ERK inhibition by low-dose 2-DG occurs independent of the growth factor used to stimulate endothelial cells suggests that 2-DG, either alone, or in combination, may effectively overcome anti-VEGF resistance in patients treated with these agents. Second, the concentrations of 2-DG used to downregulate endothelial ERK and AKT and induce ER stress are clinically achievable and manifold lower than those needed to induce tumor cell cytotoxicity. A phase I trial of this drug in combination with chemotherapy (40) showed that plasma concentrations of 2-DG after oral administration are within the range of the concentrations we used (0.6 mmol/L) to inhibit angiogenesis *in vitro*. This provides a rationale to further develop 2-DG using schedules and modes of administration that reach antiangiogenic concentrations, alone and in combination with other targeted agents. Finally, results from the current study should extend beyond 2-DG. The finding that endothelial cells do not adapt well to ER stress, leading to apoptosis, and the characterization of the pathways involved, can be used to identify agents that may mimic the effects of 2-DG and used as novel antiangiogenics. Several compounds that have been found to be antiangiogenic, such as proteasome inhibitors, tunicamycin, HIV protease inhibitors, and statins (at high doses) may mimic some of the effects of 2-DG, either by interfering with glycosylation, or directly inducing ER stress (50–54). Our data, therefore, may provide insight into the potential antiangiogenesis mechanisms of the above agents.

In summary, our studies indicate that the antiangiogenic effects of low-dose 2-DG are mediated by its inhibition of N-linked glycosylation, resulting in ERK and AKT downregulation by mechanisms including VEGF receptor hypoglycosylation and induction of endothelial ER stress, leading to GSK3β activation and apoptosis. Further investigation appears to be warranted to further develop 2-DG as an antitumor antiangiogenic agent, and to identify drugs that mimic its mechanism of action, to improve the efficacy of, and overcome resistance to currently available anti-VEGF agents.

Disclosure of Potential Conflicts of Interest

No potential conflicts of interest were disclosed.

Authors' Contributions

Conception and design: K. Kovacs, D.G. Pham, T.G. Murray, T.J. Lampidis, J.R. Merchan

Development of methodology: K. Kovacs, H. Liu, T.G. Murray, T.J. Lampidis, J.R. Merchan

Acquisition of data (provided animals, acquired and managed patients, provided facilities, etc.): K. Kovacs, C. Decatur, D.G. Pham, H. Liu, Y. Jing, T.G. Murray, T.J. Lampidis

Analysis and interpretation of data (e.g., statistical analysis, biostatistics, computational analysis): K. Kovacs, C. Decatur, M. Toro, D.G. Pham, H. Liu, Y. Jing, T.G. Murray, T.J. Lampidis, J.R. Merchan

Writing, review, and/or revision of the manuscript: K. Kovacs, C. Decatur, D.G. Pham, T.J. Lampidis, J.R. Merchan

Administrative, technical, or material support (i.e., reporting or organizing data, constructing databases): T.J. Lampidis

Study supervision: T.J. Lampidis, J.R. Merchan

Grant Support

This work was supported by grants from Sylvester Comprehensive Cancer Center (to J.R. Merchan, T.J. Lampidis, T.G. Murray: PAP Corps. J.R. Merchan, T.J. Lampidis), as well as Women's Cancer Association and the National Institutes of Health (1R01CA149659-01) to J.R. Merchan.

The costs of publication of this article were defrayed in part by the payment of page charges. This article must therefore be hereby marked *advertisement* in accordance with 18 U.S.C. Section 1734 solely to indicate this fact.

Received May 16, 2014; revised October 2, 2015; accepted October 19, 2015; published OnlineFirst December 4, 2015.

References

1. Folkman J. Angiogenesis: an organizing principle for drug discovery? Nat Rev Drug Discov 2007;6:273–86.
2. Boere IA, Hamberg P, Sleijfer S. It takes two to tango: combinations of conventional cytotoxics with compounds targeting the vascular endothelial growth factor-vascular endothelial growth factor receptor pathway in patients with solid malignancies. Cancer Sci 2010;101:7–15.
3. Hurwitz H, Fehrenbacher L, Novotny W, Cartwright T, Hainsworth J, Heim W, et al. Bevacizumab plus irinotecan, fluorouracil, and leucovorin for metastatic colorectal cancer. N Engl J Med 2004;350:2335–42.
4. Motzer RJ, Rini BI, Bukowski RM, Curti BD, George DJ, Hudes GR, et al. Sunitinib in patients with metastatic renal cell carcinoma. JAMA 2006;295:2516–24.
5. Sandler A, Gray R, Perry MC, Brahmer J, Schiller JH, Dowlati A, et al. Paclitaxel-carboplatin alone or with bevacizumab for non-small-cell lung cancer. N Engl J Med 2006;355:2542–50.
6. Rini BI, Atkins MB. Resistance to targeted therapy in renal-cell carcinoma. Lancet Oncol 2009;10:992–1000.
7. Bhatt RS, Wang X, Zhang L, Collins MP, Signoretti S, Alsop DC, et al. Renal cancer resistance to antiangiogenic therapy is delayed by restoration of angiostatic signaling. Mol Cancer Ther 2010;9:2793–802.
8. Casanovas O, Hicklin DJ, Bergers G, Hanahan D. Drug resistance by evasion of antiangiogenic targeting of VEGF signaling in late-stage pancreatic islet tumors. Cancer Cell 2005;8:299–309.
9. Pennacchietti S, Michieli P, Galluzzo M, Mazzone M, Giordano S, Comoglio PM. Hypoxia promotes invasive growth by transcriptional activation of the met protooncogene. Cancer Cell 2003;3:347–61.
10. Merchan JR PH, Qin R, Liu G, Fitch TR, Maples WJ, Picus J, et al. Final phase II safety and efficacy results of study MC0452: phase I/II trial of CCI 779 and bevacizumab in advanced renal cell carcinoma. J Clin Oncol 29, 2011 (suppl; abstr 4548).
11. Motzer RJ, Escudier B, Oudard S, Hutson TE, Porta C, Bracarda S, et al. Efficacy of everolimus in advanced renal cell carcinoma: a double-blind, randomised, placebo-controlled phase III trial. Lancet 2008; 372:449–56.
12. Rini BI, Wilding G, Hudes G, Stadler WM, Kim S, Tarazi J, et al. Phase II study of axitinib in sorafenib-refractory metastatic renal cell carcinoma. J Clin Oncol 2009;27:4462–8.
13. Datema R, Schwarz RT. Interference with glycosylation of glycoproteins. Inhibition of formation of lipid-linked oligosaccharides *in vivo*. Biochem J 1979;184:113–23.
14. Kurtoglu M, Maher JC, Lampidis TJ. Differential toxic mechanisms of 2-deoxy-D-glucose versus 2-fluorodeoxy-D-glucose in hypoxic and normoxic tumor cells. Antioxid Redox Signal 2007;9:1383–90.
15. Merchan JR, Kovacs K, Railsback JW, Kurtoglu M, Jing Y, Pina Y, et al. Antiangiogenic activity of 2-deoxy-D-glucose. PLoS ONE 2010;5: e13699.
16. Kurtoglu M, Gao N, Shang J, Maher JC, Lehrman MA, Wangpaichitr M, et al. Under normoxia, 2-deoxy-D-glucose elicits cell death in select tumor types not by inhibition of glycolysis but by interfering with N-linked glycosylation. Mol Cancer Ther 2007;6:3049–58.
17. Maher JC, Savaraj N, Priebe W, Liu H, Lampidis TJ. Differential sensitivity to 2-deoxy-D-glucose between two pancreatic cell lines correlates with GLUT-1 expression. Pancreas 2005;30:e34–9.
18. Maher JC, Wangpaichitr M, Savaraj N, Kurtoglu M, Lampidis TJ. Hypoxia-inducible factor-1 confers resistance to the glycolytic inhibitor 2-deoxy-D-glucose. Mol Cancer Ther 2007;6:732–41.
19. Chan B, Merchan JR, Kale S, Sukhatme VP. Antiangiogenic property of human thrombin. Microvasc Res 2003;66:1–14.
20. Merchan JR, Chan B, Kale S, Schnipper LE, Sukhatme VP. *In vitro* and *in vivo* induction of antiangiogenic activity by plasminogen activators and captopril. J Natl Cancer Inst 2003;95:388–99.
21. Jockovich ME, Bajenaru ML, Pina Y, Suarez F, Feuer W, Fini ME, et al. Retinoblastoma tumor vessel maturation impacts efficacy of vessel targeting in the LH(BETA)T(AG) mouse model. Invest Ophthalmol Vis Sci 2007;48:2476–82.
22. Jockovich ME, Murray TG, Escalona-Benz E, Hernandez E, Feuer W. Anecortave acetate as single and adjuvant therapy in the treatment of retinal tumors of LH(BETA)T(AG) mice. Invest Ophthalmol Vis Sci 2006;47:1264–8.
23. Jockovich ME, Suarez F, Alegret A, Pina Y, Hayden B, Cebulla C, et al. Mechanism of retinoblastoma tumor cell death after focal chemotherapy, radiation, and vascular targeting therapy in a mouse model. Invest Ophthalmol Vis Sci 2007;48:5371–6.
24. Martinet W, Abbeloos V, Van Acker N, De Meyer GR, Herman AG, Kockx MM. Western blot analysis of a limited number of cells: a valuable adjunct to proteome analysis of paraffin wax-embedded, alcohol-fixed tissue after laser capture microdissection. J Pathol 2004;202:382–8.
25. Mavria G, Vercoulen Y, Yeo M, Paterson H, Karasarides M, Marais R, et al. ERK-MAPK signaling opposes Rho-kinase to promote endothelial cell survival and sprouting during angiogenesis. Cancer Cell 2006;9:33–44.
26. Shiojima I, Walsh K. Role of Akt signaling in vascular homeostasis and angiogenesis. Circ Res 2002;90:1243–50.
27. Yang B, Cao DJ, Sainz I, Colman RW, Guo YL. Different roles of ERK and p38 MAP kinases during tube formation from endothelial cells cultured in 3-dimensional collagen matrices. J Cell Physiol 2004; 200:360–9.
28. Takahashi T, Shibuya M. The 230 kDa mature form of KDR/Flk-1 (VEGF receptor-2) activates the PLC-gamma pathway and partially induces mitotic signals in NIH3T3 fibroblasts. Oncogene 1997;14: 2079–89.
29. Hicklin DJ, Ellis LM. Role of the vascular endothelial growth factor pathway in tumor growth and angiogenesis. J Clin Oncol 2005;23:1011–27.
30. Klausner RD, Donaldson JG, Lippincott-Schwartz J. Brefeldin A: insights into the control of membrane traffic and organelle structure. J Cell Biol 1992;116:1071–80.
31. Srinivasan S, Ohsugi M, Liu Z, Fatrai S, Bernal-Mizrachi E, Permutt MA. Endoplasmic reticulum stress-induced apoptosis is partly mediated by reduced insulin signaling through phosphatidylinositol 3-kinase/Akt and increased glycogen synthase kinase-3beta in mouse insulinoma cells. Diabetes 2005;54:968–75.

32. Song L, De Sarno P, Jope RS. Central role of glycogen synthase kinase-3beta in endoplasmic reticulum stress-induced caspase-3 activation. J Biol Chem 2002;277:44701–8.
33. Meares GP, Mines MA, Beurel E, Eom TY, Song L, Zmijewska AA, et al. Glycogen synthase kinase-3 regulates endoplasmic reticulum (ER) stress-induced CHOP expression in neuronal cells. Exp Cell Res 2011;317:1621–8.
34. Wang Q, Zhou Y, Wang X, Evers BM. Glycogen synthase kinase-3 is a negative regulator of extracellular signal-regulated kinase. Oncogene 2006;25:43–50.
35. Chen CH, Shaikenov T, Peterson TR, Aimbetov R, Bissenbaev AK, Lee SW, et al. ER stress inhibits mTORC2 and Akt signaling through GSK-3beta-mediated phosphorylation of rictor. Sci Signal 2011;4:ra10.
36. Hughes K, Nikolakaki E, Plyte SE, Totty NF, Woodgett JR. Modulation of the glycogen synthase kinase-3 family by tyrosine phosphorylation. EMBO J 1993;12:803–8.
37. De Bock K, Georgiadou M, Carmeliet P. Role of endothelial cell metabolism in vessel sprouting. Cell Metab 2013;18:634–47.
38. Fraisl P, Baes M, Carmeliet P. Hungry for blood vessels: linking metabolism and angiogenesis. Dev Cell 2008;14:313–4.
39. Mohanti BK, Rath GK, Anantha N, Kannan V, Das BS, Chandramouli BA, et al. Improving cancer radiotherapy with 2-deoxy-D-glucose: phase I/II clinical trials on human cerebral gliomas. Int J Radiat Oncol Biol Phys 1996;35:103–11.
40. Raez LE, Papadopoulos K, Ricart AD, Chiorean EG, Dipaola RS, Stein MN, et al. A phase I dose-escalation trial of 2-deoxy-D-glucose alone or combined with docetaxel in patients with advanced solid tumors. Cancer Chemother Pharmacol 2013;71:523–30.
41. Stein M, Lin H, Jeyamohan C, Dvorzhinski D, Gounder M, Bray K, et al. Targeting tumor metabolism with 2-deoxyglucose in patients with castrate-resistant prostate cancer and advanced malignancies. Prostate 2010; 70:1388–94.
42. Gupta K, Kshirsagar S, Li W, Gui L, Ramakrishnan S, Gupta P, et al. VEGF prevents apoptosis of human microvascular endothelial cells via opposing effects on MAPK/ERK and SAPK/JNK signaling. Exp Cell Res 1999; 247:495–504.
43. Nakagami H, Morishita R, Yamamoto K, Taniyama Y, Aoki M, Matsumoto K, et al. Mitogenic and antiapoptotic actions of hepatocyte growth factor through ERK, STAT3, and AKT in endothelial cells. Hypertension 2001;37:581–6.
44. Zhong D, Xiong L, Liu T, Liu X, Chen J, Sun SY, et al. The glycolytic inhibitor 2-deoxyglucose activates multiple prosurvival pathways through IGF1R. J Biol Chem 2009;284:23225–33.
45. Nacev BA, Grassi P, Dell A, Haslam SM, Liu JO. The antifungal drug itraconazole inhibits vascular endothelial growth factor receptor 2 (VEGFR2) glycosylation, trafficking, and signaling in endothelial cells. J Biol Chem 2011;286:44045–56.
46. Chen R, Li J, Feng CH, Chen SK, Liu YP, Duan CY, et al. c-Met function requires N-linked glycosylation modification of pro-Met. J Cell Biochem 2013;114:816–22.
47. Contessa JN, Bhojani MS, Freeze HH, Rehemtulla A, Lawrence TS. Inhibition of N-linked glycosylation disrupts receptor tyrosine kinase signaling in tumor cells. Cancer Res 2008;68:3803–9.
48. Feige JJ, Baird A. Glycosylation of the basic fibroblast growth factor receptor. The contribution of carbohydrate to receptor function. J Biol Chem 1988;263:14023–9.
49. Kim HS, Skurk C, Thomas SR, Bialik A, Suhara T, Kureishi Y, et al. Regulation of angiogenesis by glycogen synthase kinase-3beta. J Biol Chem 2002;277:41888–96.
50. Banerjee A, Lang JY, Hung MC, Sengupta K, Banerjee SK, Baksi K, et al. Unfolded protein response is required in nu/nu mice microvasculature for treating breast tumor with tunicamycin. J Biol Chem 2011;286: 29127–38.
51. Abcouwer SF, Marjon PL, Loper RK, Vander Jagt DL. Response of VEGF expression to amino acid deprivation and inducers of endoplasmic reticulum stress. Invest Ophthalmol Vis Sci 2002;43:2791–8.
52. Dulak J, Jozkowicz A. Anti-angiogenic and anti-inflammatory effects of statins: relevance to anti-cancer therapy. Curr Cancer Drug Targets 2005;5:579–94.
53. Roccaro AM, Hideshima T, Raje N, Kumar S, Ishitsuka K, Yasui H, et al. Bortezomib mediates antiangiogenesis in multiple myeloma via direct and indirect effects on endothelial cells. Cancer Res 2006; 66:184–91.
54. Sgadari C, Barillari G, Toschi E, Carlei D, Bacigalupo I, Baccarini S, et al. HIV protease inhibitors are potent anti-angiogenic molecules and promote regression of Kaposi sarcoma. Nat Med 2002;8:225–32.